

Full title: “Consistency test of precipitating ice cloud retrieval properties obtained from the observations of different instruments operating at Dome-C (Antarctica)”

**This is an interesting article that uses REFIR-PAD Fourier transform spectroradiometer, MMR, lidar data and particle probe imagery for four case studies of precipitating ice clouds at Dome-C, Antarctica. The REFIR-PAD data are forward modeled to retrieve microphysical properties of the clouds, and then the results are compared to the MRR reflectivity data. The methodology described in this article provides ground-truth for satellite-based retrievals of ice cloud properties in Antarctica. I recommend considering my comments and modify the article appropriately before the article is accepted.**

## Main Comments

**1. I'd like to see a sounding, or at the minimum, discussing the temperatures sampled for each of the four cases. This should be done in the abstract as well as in the body of the text.**

We thank the reviewer for the constructive comments and advises, which allowed improving the quality of both our analysis and the manuscript. We tried to address all requests.

The temperature profile during the precipitation events usually varied from  $-20\text{ }^{\circ}\text{C}$  to  $-40\text{ }^{\circ}\text{C}$ . The average temperature obtained by weighting the retrieved profiles over the entire dataset with the corresponding backscattering lidar signal was found equal to  $-28\text{ }^{\circ}\text{C}$ . We showed in Fig. 1 the plot of four retrieved profiles of temperature (colored lines on the left panel) at the dates reported in the label. We can see the inversion of the temperature, typical of the Antarctic Plateau, at around 750 m above the ground, while the strong peak at the very first layers corresponds to the internal temperature of the REFIR-PAD instrument, since this latter was treated as a separated environment in the retrieval procedure as also mentioned in the text. We can also see that only on 21/04/2020 the inversion of the temperature reached the  $-6\text{ }^{\circ}\text{C}$  at around 1000 m.

On the right panel, we have also reported the backscattering lidar profiles, which show that the precipitating clouds occurred below 500 m, so that the average temperature weighted with the lidar signal turned out being equal to  $-30\text{ }^{\circ}\text{C}$  on the days 23/02, 24/02 and 23/04, while it rised up to  $-25\text{ }^{\circ}\text{C}$  on the day 21/04.

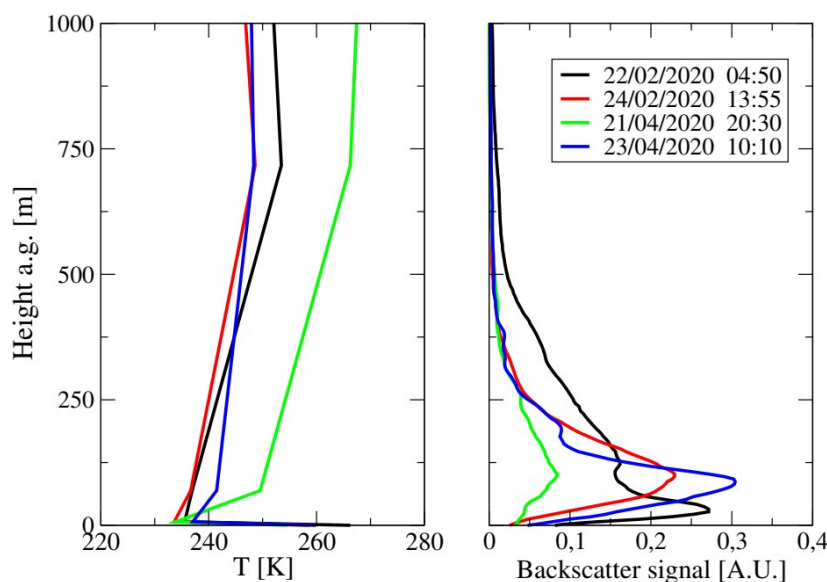


*Figure 1. Left panel: retrieved temperature profiles corresponding to the selected days of measurement. Right panel: backscattering lidar signals in arbitrary units for the analysed measurements.*

The average temperature values and Fig. 1 were both added in the abstract on line 9: “*The retrieved effective sizes and optical depths varies on average in the range 100 - 200  $\mu\text{m}$  and 0.1 - 5, respectively. The average in-cloud retrieved temperature over all dataset was found to be -28  $^{\circ}\text{C}$ ”.*

The following sentence was added to the text at line 339 : “*The retrieved effective diameters mostly varied in the range 100-200  $\mu\text{m}$ , while the retrieved optical depth between 0.1-5 over all dataset. From the retrieved temperature profiles we assessed the average in-cloud temperatures by weighting the profiles with the corresponding backscattering lidar signals. The temperature varied between -20  $^{\circ}\text{C}$  and -40  $^{\circ}\text{C}$  and on average was equal to -28  $^{\circ}\text{C}$ . Specifically for the cases discussed hereafter, the average temperatures turned out to be -30  $^{\circ}\text{C}$  on the days 23/02, 24/02 and 23/04, while on the day 21/04 equal to -25  $^{\circ}\text{C}$ ”.*

Daily radiosondes were routinely launched at Concordia station at 12:00 UTC by the Italian meteo Climatological Antarctic Observatory staff. This data, since were not continuous, most of the time they were not available at the time of the REFIR-PAD measurement. However, they allowed to obtain a good climatology of the atmospheric profile used as a priori information and initial guess in the retrieval procedure.

**2. An opportunity was missed to combine the MRR and Lidar data to derive the microphysical properties of the clouds sampled, using retrieval algorithms such as 2CICE, DARDAR and its successor. As it stands, the lidar data is not used for the analysis, maybe just to determine liquid water presence (?) and for the plots shown.**

We know well the two methods mentioned by the reviewer. They exploit the synergistic combination of radar-lidar observations, but their effectiveness is limited to a radar signal at higher frequencies than that of MRR (24 GHz, K band). As far as we know, these methodologies have been largely applied only to the satellite measurements, such as CLOUDSAT-CALIPSO (DeLanoë and Hogan (2008/2010) by using the DARDAR algorithm and Deng et al. (2015) by using the 2C-ICE). In both these cases the signal of the CPR Radar at 94 GHz (W band) was exploited, which was sufficiently high to explore the smallest particles and sensitive to the top of the clouds, where no precipitation events can occur. This allows addressing stable solutions within the retrieval algorithm. In our ground-based configuration, the MRR is a radar that presents strong limits in sensitivity and furthermore is used from the ground and very close to the precipitation.

On the other hand, the backscattering-depolarization lidar installed at Dome-C provides only qualitative measurements and it also shows clear limits in the performance, in fact the generated signal turns out to be too noisy, mostly in the height near above the cloud top, to be used in any kind of retrieval algorithm, such as the Klett inversion method as we done, for example, during FIRMOS campaign at Zugspitze mount (Di Natale et al. 2021). We have already tried to apply this method in order to derive the cloud extinction profile and, thus, the optical depth, but every attempt has failed so far as expected. We added the following sentence to the text on line 271 in order to clarify this aspect: “*A direct retrieval of the optical extinction or ice fraction from the lidar measurements was not possible due to the high noise of the signal above the cloud top heights, which does not allow the application of a retrieval algorithm such as the Klett method. These lidar measurements represent qualitative data, which allow identifying the occurrence of clouds and assessing their position and the presence of ice and supercooled water.*” .

**3. You could use the lidar data in the following way. Convert backscatter to extinction. Then, use the relationship between ice water content and extinction from the following article and those used in the study: Thornberry, T. D., Rollins, A. W., Avery, M. A., Woods,**

**S., Lawson, R. P., Bui, T. V., and Gao, R.-S. (2017), Ice water content-extinction relationships and effective diameter for TTL cirrus derived from in situ measurements during ATTREX 2014, J. Geophys. Res. Atmos., 122, 4494– 4507, doi:10.1002/2016JD025948.**

As we stated by answering the previous comment, the backscattering-depolarization lidar installed at Dome-C provides qualitative measurements, which allow to well identify the occurrence of clouds and precipitation events, to derive the cloud position (top and bottom heights) and to detect the presence of supercooled liquid water. The retrieval of the extinction profile and, thus, the optical depth, as well as the ice fraction liquid/ice is quantitatively not possible to achieve by using this lidar data.

**4. The data from the ICE Camera offers an opportunity to derive particle masses from the melted diameter. The heated glass plate the particle land on provides that opportunity-initial diameter and melted diameter. The melted diameter may not be spherical but laboratory experiments could be conducted to find the relationship between melted diameter and spherical diameter.**

The ice particles never melt on the ICE-CAMERA surface, as its temperature is kept below -5 °C also during the heating of the plate. Sublimation occurs without melting. This information was added to the text.

**5. The Doppler velocity data from MRR could be used to derive the median mass diameter.**

Median mass diameter could be inferred from Doppler velocity observations by MRR, but this requires a relationship between diameters and velocities of the falling particles. While this relationship is relatively fixed for liquid precipitation (and MRR exploits it to obtain DSDs for each probed height during rainfall), the solid hydrometeors can follow different v-D relationships due to their sizeable microphysical variability (habits, shapes, orientation, fall behavior, and density).

As a follow-on of this article, we plan to combine radiometer and MRR Doppler data to achieve a v-D relationship (or more relationships) suited for DC precipitation, even combining observations from the ICE-CAMERA and from a disdrometer to be installed soon. Nevertheless, this analysis needs more snowfall data to make the finding more robust. This is the reason why we have not derived particle diameters from MRR data at this stage, but this analysis will be performed in a future work.

**6. The PSD dispersion is given as 7 on line 138. I suggest using a temperature-dependent dispersion, such as given in the article Ice Cloud Particle Size Distributions and Pressure-Dependent Terminal Velocities from In Situ Observations at Temperatures from 0 to -86C by .**

We are grateful to the reviewer for this hint.

Referring to the paper Heymsfield et al. (2002, 2013), Wolf et al. (2019) and Jackson et al. (2015) (all these references were added to the manuscript), according to the range of temperature found at Dome-C from our analysis, between -50 and -25 °C, the values of the corresponding  $\mu$  coefficient of the PSD should span between 0 and 2.

From a radiometric point of view, as already discussed in Wyser and Yang (1998), if we have defined the effective diameter as in Eq. (2) in the text, the spectral radiance turns out to be insensitive to the detailed shape of the size distribution, in particular to the dispersion coefficient  $\mu$ . We showed in Fig. 2 the plots of the differences between the spectral radiances simulated with SACR by placing ice clouds from the ground up to 5 km of absolute height with optical depths 0.2, 0.8, 1.5 and 4, and effective diameters equal to 100 and 200  $\mu\text{m}$ , as they cover the range of values found; simulations were performed by averaging the single scattering properties provided by the

Ping Yang database by using three different dispersion coefficients  $\mu$ , namely 0, 2 and 7. In red are shown the differences between the radiances simulated with  $\mu = 0$  and  $\mu = 7$  (the value used in our analysis), rather in green are shown the differences between the radiances simulated with  $\mu = 2$  and  $\mu = 7$ . The black curves represent the REFIR-PAD spectral noise. We can see that the differences are well inside the noise also in the far infrared (FIR), though downwelling spectral radiance is not sensitive to the detailed shape of the PSD, and the value of  $\mu$  does not affect the results of the cloud parameters retrieval.

We added the following sentence to the text on line 143: “As long as the effective diameter is defined as in Eq. 2, the spectral radiance detected by REFIR-PAD turns out to be insensitive to the detailed shape of the size distribution, in particular to the dispersion coefficient  $\mu$ . We also verified this assertion by performing simulations of the downwelling spectral radiance for different values of  $D_{ei}$  and  $OD_i$  by assuming different values of  $\mu$  between 0 and 7 to generate the crystal infrared optical properties. So that the results of the cloud properties retrieval can not be affected by the choice of  $\mu$ .”.

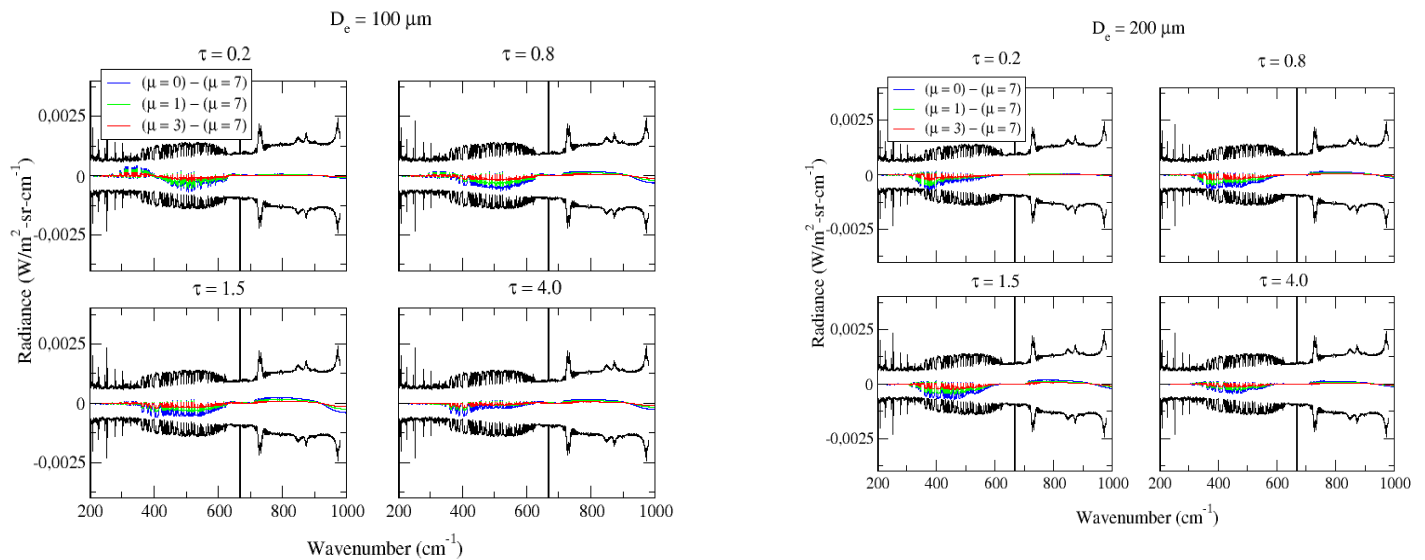


**Figure 2.** Differences of the spectral radiances simulated with SACR by placing a precipitating ice cloud from the ground (3.233 km) up to 5 km of absolute height with optical depths 0.2, 0.8, 1.5 and 4, and effective diameters equal to 100  $\mu\text{m}$  (left plot) and 200  $\mu\text{m}$  (right plot); the single scattering properties provided by the Ping Yang et al. (2013) database were averaged by using three four dispersion coefficients, 0, 1, 3 and 7. The differences between radiances obtained with  $\mu = 0$  and  $\mu = 7$  are represented by the blue curves, the differences between  $\mu = 1$  and  $\mu = 7$  are indicated by the green curves and those between  $\mu = 3$  and  $\mu = 7$  are reported in red. In black the REFIR-PAD spectral noise is also reported.

We can conclude that the coefficient  $\mu$  does not affect the retrieval results of cloud parameters  $OD_i$  and  $D_{ei}$ . However, the intercept  $N_0$  change a little and was recalculated by using Eq. 9 and expressed in  $\text{cm}^{-5}$  to compare it with the results by Heymsfield et al. (2002) and (2013). As a consequence, also the values of  $Z_e$  from Eq. 23 were updated. We also have updated Fig. 11. The values of  $N_0$  and the slope  $\Lambda = (\mu+3)/L_m$  were shown in the new plots of Fig. 14 as a function of the cloud temperature  $T_{\text{cld}}$ . The  $N_0$  values varies between  $10^{-2}$  and  $10^4$ , while  $\Lambda$  between 20 and 200  $\text{cm}^{-1}$ ; these values turn out to be in very good agreement with the distributions found both in Heymsfield et al. (2002) and (2013).

We have replaced Table 1 with another one indicating only the habit indices need for interpreting the plot in the added figure (Fig. 12) reported below.

“In Fig. 3 below (now Fig. 12 in the text), in the upper panel were reported the reduced  $\chi^2_{red}$  obtained from the  $Z_e$  retrieved from REFIR-PAD and those measured by the MRR by assuming  $\mu = 0,1,2$  (green, blue, red curves); in the lower panel are shown the total number of measurements (N) available considering the cut off at -5 dBZ. On the x-axis we reported the habit index explained in Table 1. To select the best habits we adopted the criteria of having the  $\chi^2_{red}$  close to 1 and maximize the number of measurements (N) by assuming some thresholds (dashed black lines in Fig. 3): we required that N had to be greater than 25 and  $\chi^2_{red}$  had to stay between 0.5 and 2, since when it decreases too much usually indicates that the error is overestimated. The selected cases that complied the criteria were identified with cyan triangles.

From Fig. 3 we can see that there is no much difference by varying  $\mu$  in the range 0-2 for the selected cases, so that we assumed as average value  $\mu = 1$  for the next considerations.

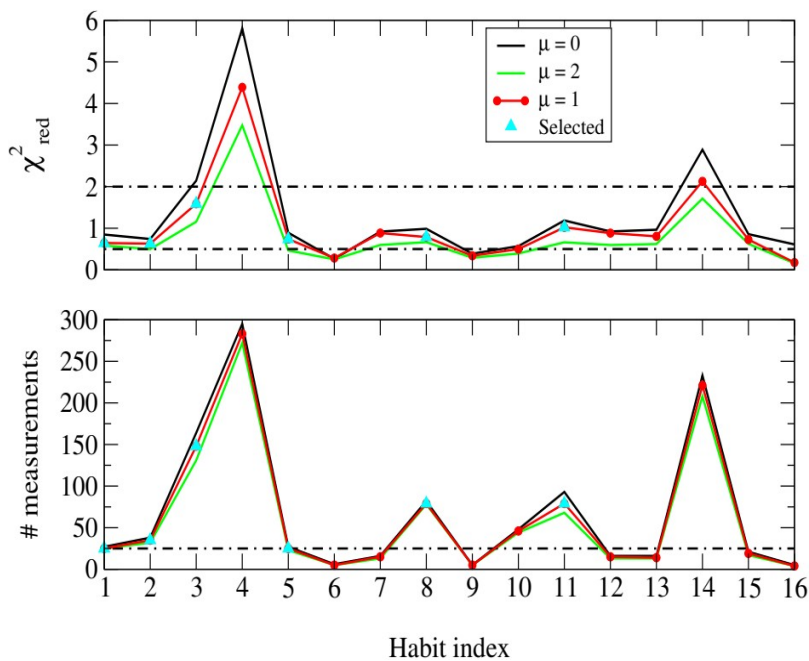


*Figure 3. Upper panel: reduced  $\chi^2_{red}$  calculated from the  $Z_e$  retrieved from REFIR-PAD and those measured by the MRR by assuming  $\mu = 0,1,2$  (green, blue, red curves). Lower panel: number of measurements above the -5 dBZ threshold assumed for the analysis.*

The habits that showed best accordance with the radar measurements were the 5/6 branches bullet rosettes, the thin and long columns and the 8-columns/large block aggregates. Fig. 4 (now Fig. 13 in the text) shows the comparison of the MRR measured reflectivity with those obtained from REFIR-PAD by using some of the habits from the EMD (Eriksson Microwave Database) in Table 1 that provided the best agreement.

The high occurrence of hexagonal columns, aggregates and bullet rosettes was confirmed by the ICE-CAMERA photographs. In particular, the high occurrence of hexagonal columns was corroborated by the presence of  $22^\circ$  halos detected by the colocated HALO-CAMERA sky images as shown in previous studies at South Pole by Lawson et al. (2006).

It also should be noted that while the correlation coefficient turned out to be moderate (maximum  $\sim 0.3$ ), this was mostly due to the difficulty of retrieving with good accuracy the shape of the PSD from the FIR observations, and in particular the intercept  $N_0$ , for large particle sizes, and mostly because of the need of increasing the number of measurements for improving the statistical distribution.

However, the results indicate that in the particle size range between about 600 and 2000  $\mu\text{m}$ , the retrieval algorithm was able to estimate the intercept assuming the dispersion coefficient  $\mu$  in the range 0-2, as shown in Fig. 4. The distributions of the retrieved  $N_0$  converted in  $\text{cm}^{-5}$  and the slope  $\Lambda = (3+\mu)/L_m$  in  $\text{cm}^{-1}$  as a function of the retrieved cloud temperature ( $T_{\text{cld}}$ ), were found in very good accordance with those found in Heymsfield et al. (2013, 2002) and Wolf et al. (2019) and they were shown in Fig. 4, left and right panels, respectively. Note that  $N_0$  varied mostly between  $10^2 - 10^4 \text{ cm}^{-5}$ , while  $\Lambda$  mostly between 20-200  $\text{cm}^{-1}$ . The average relative error found for  $N_0$  was equal to 20%, which was comparable to the systematic error due to the assumption of a specific habit in the retrieval as shown in Fig. 7.”

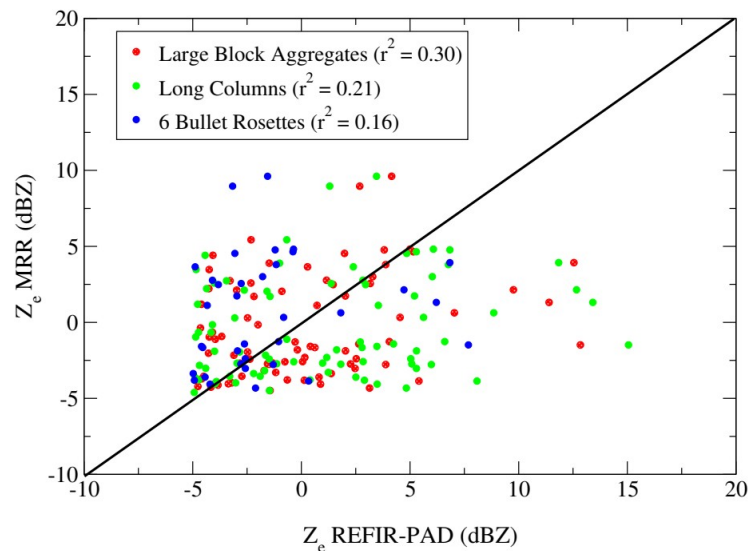


*Figure 4. Scatter-plots of the  $Z_e$  measured by the MRR and those retrieved from REFIR-PAD by assuming  $\mu = 1$  and by using the habits from Eriksson et al. (2018) database that provided the best accordance: long columns, large plates aggregates and 6 bullet rosettes.*

This results and updates were added in the text, abstract and conclusions.

## Minor Comments

**Reviewer R1 has noted improvements to the figures that should be made.**

Yes, all the requests have been addressed.

**Line 101. What are the minimum and maximum altitudes sampled by the MRR.**

We have set MRR with 40 m as height resolution, so the sampled range goes from 40 to 1240 m. However, the first two range gates are usually excluded as they are affected by near-field effects, likewise the last range gate due to the low SNR. So, the actual MRR altitude range is 120-1200 m.

**102-103. What are the minimum and maximum reflectivities that can be measured by MRR?**

The manufacturer indicates -2 dBZ as the minimum detectable reflectivity for MRR. In this work, we have applied the Maahn and Kollias' (2012) routine to MRR raw data to improve MRR

sensitivity measurements in case of snow. According to them this routine increases MRR sensitivity to  $-14$  and  $-8$  dBZ, depending on the vertical range bin. However, we discarded reflectivity values lower than  $-5$  dBZ from the analysis since, below that threshold, MRR measurements could be incomplete. So we have adopted a very conservative threshold to preserve MRR data's reliability in a very challenging site such as Dome-C.

**138-139. Compare your sigma and mu values to those observed for cirrus clouds.**

Within the REFIR-PAD retrieval procedure, we assumed a PSD with a dispersion coefficient  $\mu$  given by the relation  $\mu = 7$ . This was assumed in previous work in the Arctic and in Antarctica, since there are no sufficient measurements in the latter place. However, following the reviewer advice, we reconsidered values of  $\mu$  coefficient according to the statistical relationship with the cloud temperature as discussed in Heymsfield et al. (2013, 2002), using the values 0, 1 and 2 to calculate the  $N_0$  and the radar reflectivity  $Z_e$  as provided in the mentioned works for temperatures between  $-25$  and  $-50$  °C. The retrieval products were not affected by changing  $\mu$ , since the downwelling infrared spectrum is not sensitive to this parameter as shown in the Fig. 1. We added the plots in Fig. 5 (now Fig. 14 in the text) of the  $N_0$  expressed in  $\text{cm}^{-5}$  and the slope  $\Lambda$  in  $\text{cm}^{-1}$  as a function of the cloud temperature ( $T_{\text{cld}}$ ) to compare them with the results shown in Heymsfield et al. (2013, 2002) and Wolf et. Al (2019), finding a good accordance for our range of temperature.

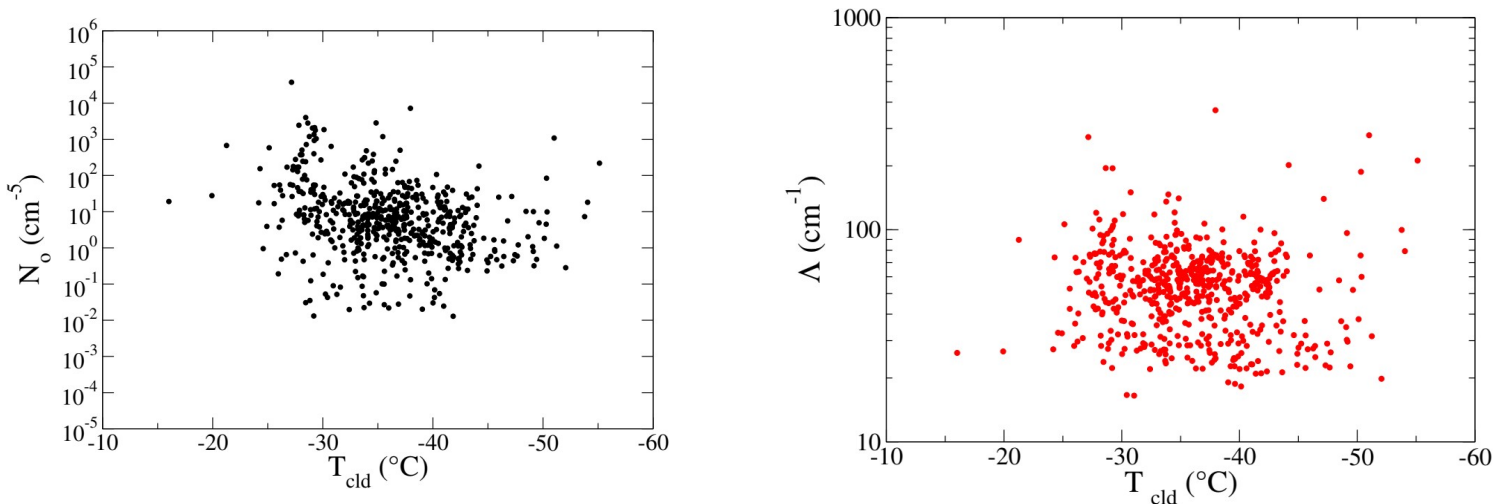


*Figure 5. Left and right panels: intercept  $N_0$  and slope  $\Lambda$  as a function of the cloud retrieved temperature ( $T_{\text{cld}}$ ).*

**164: "to us"**

Corrected in the text.

**166: Specifically, what are the temperatures of the clouds studied here.**

The average cloud temperature was calculated by averaging the retrieved temperature profiles inside the cloud top and bottom weighted with the corresponding lidar signals and it was found equal to  $-28$  °C. We added this value in the text.

**216: How is liquid water detected from your instruments.**

The liquid water and ice water path could be derived from the REFIR-PAD retrieval products by using Eq. (7) for water and ice.

Mixed-phase clouds appeared above the site on 23 February between 8-9 UTC and 12-13 UTC, where the presence of supercooled water was detected by the depolarization signal at around 200 m above the ground. In the first mixed-phase cloud time slot, the retrieval provided an average ice fraction  $\gamma$  equal to 0.47 with liquid water path equal to 0.62 g/m<sup>2</sup>, while in the second time mixed-phase slot values were equal to 0.56 and 1.5 g/m<sup>2</sup>.

On 21 April, a mixed-phase cloud with supercooled water occurred between 17 and 20 UTC at about 1500 and 400 m above the ground. In this case  $\gamma$  was found on average equal to 0.58 and LWP equal to 9.5 g/m<sup>2</sup>.

These sentences were added to the text at lines 354 and 364, respectively.

On the advice of reviewer 1 we also expanded the discussion about the results shown in section 4.3.

## **262. You have particle imagery to characterize the particle habit(s). How does this compare to the particle types interpreted from the analysis.**

The retrieval from REFIR-PAD infrared spectral radiances allowed to assess the  $D_e$  and, thus, the modal radius  $L_m$  of the PSD, which represents the main parameter to which the downwelling radiance turns out be sensitive. The other important parameter, the intercept  $N_o$ , was also derived from both the  $D_e$  and the optical depth  $OD_i$ . The cloud parameters retrieval from the REFIR-PAD infrared spectra is not affected by the specific value of  $\mu$ , in fact the infrared downwelling spectral radiance is insensitive to it as the effective diameter is defined as in Eq. (2). To calculate the  $N_o$  from Eq. (9), we assumed  $\mu = 1$  and then we calculated the reflectivity. Retrieved reflectivity fit well the radar data even though a moderate spread occurs because of the difficult to precisely estimate the PSD parameters due to the assumption of homogeneous vertical size and habit distribution along the precipitating cloud and because more data need to be collected for improving the statistics. The photographs of the ICE-CAMERA clearly show the presence of estimated columns and aggregates in the cases 23-24 February (Figs. 18 and 20 in the text), while some bullet rosettes appear on 24 February at 8:00 UTC (Fig. 19 in the text). The figures of the ICE-CAMERA photographs were updated, as also requested by the reviewer 1: they were enlarged and we added the zoom on specific ice crystals.

## **310: "provided" to "provide"**

Corrected in the text.

## **320: Specifically, what were the measured in-cloud temperatures?**

We added in the text the values of the mean in-cloud temperature over all dataset, found equal to -28 °C, and the specific values corresponding to the four selected cases.

## **Figure 11: To me, the relationship between $Z_e$ measured by MRR and that retrieved does not look very good. MRR reflectivities are quite flat whereas those from REFIR-PAD vary quite a bit.**

As we already stated, the sensitivity of the MRR is pretty low to the ice crystals occurring at Dome-C, in fact it allows to detect only the larger particles. The PSD retrieved from REFIR-PAD measurements describes an average distribution of the particle sizes over all the precipitating clouds, which can turn out being affected by a large error. For this reason, we are aware that even though the retrieved points stay along the median line, a wide spread occurs between the data, indicating a moderate correlation index, as stated in the text. However, the fact that the values of the calculated  $Z_e$  and those measured by the radar are close and of the same order represents a good indicator of the



goodness of the retrieval of the PSD parameters and their consistency. Finally, we are confident that collecting more data will allow improving the correlation between the retrieved  $Z_e$  and the observed ones.

**Figures 13 and 16: Show fewer crystals in Figs. 11-12 so that they can be more easily identified by the reader**

We suppose the reviewer refers to the crystals of the ICE-CAMERA scanings in Fig. 13 and 16. In this case, we think that it would be better to split the two photographs as also suggested by the reviewer 1. In fact, we agree that some of the smallest crystals could be difficult to distinguish. Figures were separated, enlarged and we added the zoom on specific crystals.

**360, 361: remove "the" in "between the"**

Corrected in the text.

**368. It would be nice to do some combined radar/lidar analysis or lidar analysis separately.**

As discussed in the previous answers, a deeper analysis of the lidar data is not possible, since the signal turns out to be too noisy and it does not allow the application of a retrieval algorithm to derive the extinction coefficient and the optical depth. This is due to a limitation of the instrument which was made by prioritizing the compactness, portability, and durability in order to be installed in such an extreme site. For this reason, the data provided by this lidar are mostly qualitative and not quantitative. Similarly, the MRR is a compact object that exhibits clear limits in power and performance, but it also guarantees durability and reliability in such environmental conditions.

**References:**

- [1] Julien Delanoë and Robin J. Hogan, "A variational scheme for retrieving ice cloud properties from combined radar, lidar, and infrared radiometer", *Journal of Geoph. Research*, Vol. 113, D07204, doi:10.1029/2007JD009000, 2008.
- [2] Julien Delanoë and Robin J. Hogan, "Combined CloudSat-CALIPSO-MODIS retrievals of the properties of ice clouds", *Journal of Geoph. Research*, Vol. 115, D00H29, doi:10.1029/2009JD012346, 2010.
- [3] Min Deng, Gerald. G. Mace, Zhien Wang, and Elizabeth Berry, "CloudSat 2C-ICE product update with a new  $Z_e$  parameterization in lidar-only region", *Journal of Geophysical Research: Atmospheres*, Vol. 120, No. 23, doi:10.1002/2015JD023600, 2015.
- [4] Maahn, M. and Kollias, P.: Improved Micro Rain Radar snow measurements using Doppler spectra post-processing, *Atmospheric Measurement Techniques*, 5, 2661–2673, <https://doi.org/10.5194/amt-5-2661-2012>, 2012.